Check for updates

SARS-CoV-2 suppression depending on the pH of graphene oxide nanosheets†

Md. Saidul Islam, [ID] [ab] Masahiro Fukuda,[b] Md. Jakir Hossain,[cd] Nurun Nahar Rabin,[ab] Ryuta Tagawa,[a] Mami Nagashima,[e] Kenji Sadamasu,[e] Kazuhisa Yoshimura,[e] Yoshihiro Sekine, [ID] [f] Terumasa Ikeda*[d] and Shinya Hayami [ID] *[abg]

Severe acute respiratory syndrome coronavirus 2 (SARS-CoV-2) inactivation of pH-dependent graphene oxide (GO) nanosheets is presented. The observed virus inactivation using an authentic virus (Delta variant) and different GO dispersions at pH 3, 7, and 11 suggests that the higher pH of the GO dispersion yields a better performance compared to that of GO at neutral or lower pH. The current findings can be ascribed to the pH-driven functional group change and the overall charge of GO, favorable for the attachment between GO nanosheets and virus particles.

Novel coronavirus disease 2019 (COVID-19) is an infectious disease caused by the severe acute respiratory syndrome coronavirus 2 (SARS-CoV-2). SARS-CoV-2 first appeared at the end of 2019 in Wuhan, China, and still continues to show adverse impacts in terms of quality of life and worldwide economic sustainability.[1,2] This virus is believed to spread through small liquid particles ranging from large respiratory droplets to small aerosols coming from the mouth and nose when an infected person coughs, sneezes, speaks, sings, or breathes and its likelihood of spreading increases indoors and in crowded environments. Even though the vaccination process has already been applied to stop the spread of the virus, the virus has

continuously evolved with multiple mutations particularly in the spike (S) gene, which contributes to the emergence of new variants and resistance to vaccine-induced immunity. In addition, those who never develop symptoms can also pass the virus on to others, making it more complicated to prevent the virus from spreading. Therefore, the key strategies to prevent or mitigate the spread of the virus include the development of anti-SARS-CoV-2 active materials in the form of face masks and other safety equipment for use in everyday life.[3–5] In light of this, recently, our group reported the inactivation of SARS-CoV-2 using graphene oxide (GO) nanosheets along with our understanding of the SARS-CoV-2 inactivation route.[6] Particularly, the antiviral mechanism of GO nanosheets is associated with the attachment of virus particles on the GO surface through electrostatic interaction between the negatively charged GO and positively charged virus particles followed by the decomposition of viral proteins. Since the attachment of GO to the virus particles largely depends on the surface functional groups, which can be controlled using different parameters including the pH of the GO dispersion, some fundamental investigations including on the effect of pH on obtaining the optimum efficiency from GO-based anti-SARS-CoV-2 are important.

GO, a carbon-based two-dimensional (2D) material, owing to its exclusive physical and chemical properties, shows impressive potential and possibilities in materials science with a wide area of application including an anti-SARS-CoV-2 response.[7–12] The structure of GO possesses a large ratio of oxygen-containing functional groups including epoxy, hydroxyl, and carboxyl groups.[13–15] These functional groups of GO are believed to be attached to the positively charged SARS-CoV-2 viral particles and thereafter cause damage to the virus through the deactivation of the S and N (nucleocapsid) protein of the virus.[6,12] Interestingly, the functional groups of GO can be altered by changing the pH of the dispersion. In particular, the epoxy groups on the GO surface are quite stable under acidic conditions. However, under alkaline conditions, the ring-opening conversion of epoxy to hydroxyl is caused by a nucleophilic base due to the large strain of the three-membered ring of the

[a]Department of Chemistry, Faculty of Advanced Science and Technology, Kumamoto University, 2-39-1 Kurokami, Kumamoto 860-8555, Japan. E-mail: hayami@kumamoto-u.ac.jp

[b]Institute of Industrial Nanomaterials, Kumamoto University, 2-39-1 Kurokami, Chuo-ku, Kumamoto 860-8555, Japan

[c]Division of Molecular Virology and Genetics, Joint Research Center for Human Retrovirus Infection, Kumamoto University, 2-2-1 Honjo, Kumamoto 860-0811, Japan

[d]Graduate School of Medical Sciences, Kumamoto University, Kumamoto 860-0811, Japan

[e]Tokyo Metropolitan Institute of Public Health, Tokyo, Japan

[f]Priority Organization for Innovation and Excellence, Kumamoto University, 2-39-1 Kurokami, Chuo-ku, Kumamoto 860-8555, Japan

[g]International Research Center for Agricultural and Environmental Biology (IRCAEB), 2-39-1 Kurokami, Chuo-ku, Kumamoto 860-8555, Japan

† Electronic supplementary information (ESI) available. See DOI: https://doi.org/10.1039/d3na00084b
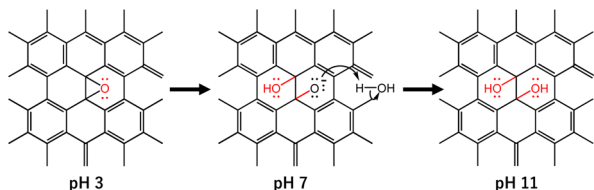
Scheme 1 Illustration of the pH-dependent functional groups change in GO.

epoxy group (Scheme 1).[16] In addition, the change in pH of the GO dispersion is associated with the change in the overall negative charge of GO. Therefore, pH-dependent GO is anticipated to show a difference in anti-SARS-CoV-2 activity. In the current work, we demonstrated the effect of pH in the GO dispersion on the inactivation of SARS-CoV-2. We have selected three different GO dispersions at pH 3, pH 7, and pH 11 which represent acidic, neutral, and basic conditions, respectively. We treated the virus stock with the pH dependent GO dispersions while keeping all other conditions unchanged. The virus inactivation was evaluated by plaque assay and enzyme-linked immunosorbent assay (ELISA) against N protein. The current study suggested that GO dispersion at higher pH shows comparatively higher anti-SARS-CoV-2 activity than that at neutral or lower pH.

GO was purchased commercially from Nippon Shokubai Co with an oxidation degree of 33% and used without further purification. The pH of GO was adjusted to the values of 3, 7, and 11 using the appropriate amounts of HCl and ammonia solution. GO at pH 3, 7, and 11 are denoted as GO (3), GO (7) and GO (11), respectively. The prepared GO samples were characterized using FTIR, XPS, and solid-state ^{13}C-NMR analysis. The isolation and titration of the B.1.617.2/Delta variant (strain TKYTK1734; GISAID ID: EPI_ISL_2378732) has been described previously.[17] This variant was used to investigate the antiviral activity of each GO sample against SARS-CoV-2. The plaque assay and quantification of N protein by ELISA (Proteintech, cat# KE30007) were conducted in a BSL-3 room as reported previously.[6,18,19,23] The details of the experimental procedure are shown in the ESI.†

The physical and chemical properties of GO (3), GO (7) and GO (11) are shown in Fig. 1 and S1.† The optical photograph shown in Fig. S1† clearly presents a color change from brown in GO (3) to black in GO (11). The difference in the color of the GO dispersion indicates the alteration of the functional groups in GO. The changes of functional groups in GO (3) and GO (11) are compared using XPS, FTIR, and ^{13}C NMR analysis. Fig. 1a presents the deconvoluted C 1s XPS spectra of GO (3), GO (7), and GO (11). The characteristic peaks for oxygenated functional groups include hydroxyl (C–OH), epoxy (C–O–C), carbonyl (–C=O), and carboxyl (–COOH) groups with peak intensity approximately at 286.4–286.6 eV, 286.8–287.0 eV, 287.8–288.0 eV and 289.0–289.3 eV, respectively.[21] Clearly, the peak intensity at 286.8–287.0 eV corresponding to the epoxy group is much higher in GO (3) compared to that of GO (11) indicating the presence of a large number of epoxy (C–O–C) groups in GO (3).
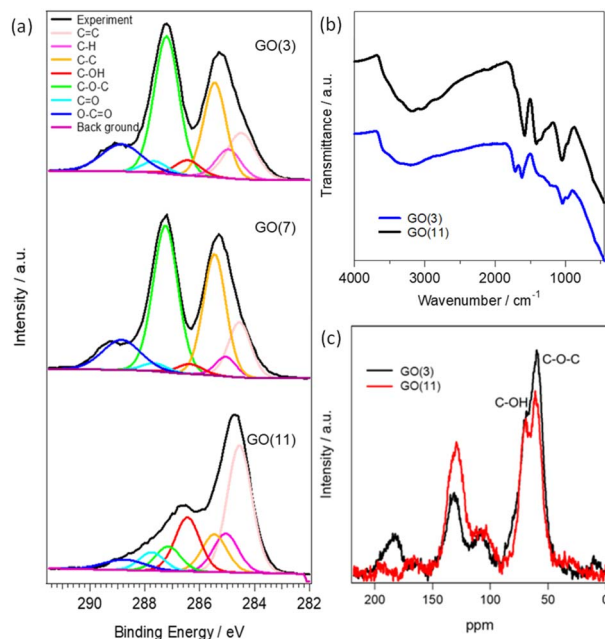

Fig. 1 Characterization of the prepared GO samples. (a) C 1s XPS spectra of GO (3) (GO at pH = 3), GO (7) (GO at pH = 7) and GO (11) (GO at pH = 11), (b) FTIR spectra GO (3) and GO (11), and (c) ^{13}C NMR spectra of GO (3) and GO (11).

On the other hand, the peak intensity in the hydroxyl group at 286.4–286.6 eV is higher in the case of pH (11) compared to that of GO (3). The observation indicates that the conversion of an epoxy to a hydroxyl group occurred during the pH change in GO. The result is further supported by using FTIR in Fig. 1b and ^{13}C NMR analysis in Fig. 1c. The FTIR spectrum of GO samples is difficult to interpret due to the overlapping bands from numerous chemical bonds. However, the characteristic FTIR peaks of GO observed at approximately 1720, 1635, 1290 and 1050 cm^{-1} correspond to the stretching frequencies of –C=O (carboxyl and carbonyl), –C=C– (aromatic sp^2 carbon), –C–O–C– (epoxy) and –COH (hydroxyl) functional groups, respectively. Moreover, the broad intense band at around 3350 cm^{-1} indicates the presence of hydroxyl groups or water molecules adsorbed on the hydrophilic functional sites of GO. Clearly, GO (11) shows higher intensities for the peaks at 3350 and 1050 cm^{-1} corresponding to the –C–OH groups while the peak intensity for the –C=O and –C–O–C– functional groups at 1720 and 1290 cm^{-1}, respectively, decreases compared to that of GO (3).

The observed spectra from solid-state ^{13}C NMR of GO (3) and GO (11) are shown in Fig. 1c. The peak intensity at 61 and 70 ppm represents the epoxides and hydroxyl functional groups, respectively.[22] The relative peak intensity for the epoxy group is larger in GO (3) compared to that of GO (11). On the other hand, the peak intensity for hydroxyl groups in GO (11) slightly increased compared to that of GO (3). This observation also indicated that the change in pH from 3 to 11 of GO dispersions is associated with the conversion of epoxy to hydroxyl groups. The conversion of epoxy to hydroxyl groups is due to pH change

in accordance with some previous reports.[16,20] In particular, the three-membered ring of the epoxy groups possesses significant structural strain, and the ring-opening conversion of the epoxy to hydroxyl is caused by a nucleophilic base. The epoxy groups readily undergo nucleophilic attack by OH^- thus relieving the strain in the three-membered rings to convert each epoxy group to a *trans-vic*-diol group *via* an S_N2 reaction.[16]

To test the variation of anti-SARS-CoV-2 activity depending on the pH of the GO dispersion, the Delta variant was used to perform plaque assay in the presence and absence of GO while keeping all other conditions unchanged. As shown in Fig. 2a and b, typical cytopathic effects were observed in the absence of GO.[6,18,19,23] The treatment of the virus stock with GO (under all pH conditions) significantly decreased the plaque-forming unit (PFU). However, a slight increase in the virus inactivation was observed for both low pH and high pH GO dispersions compared to that at pH 7 (Fig. 2b). The antiviral behaviour shows an increasing order of GO (7) < GO (3) < GO (11). To
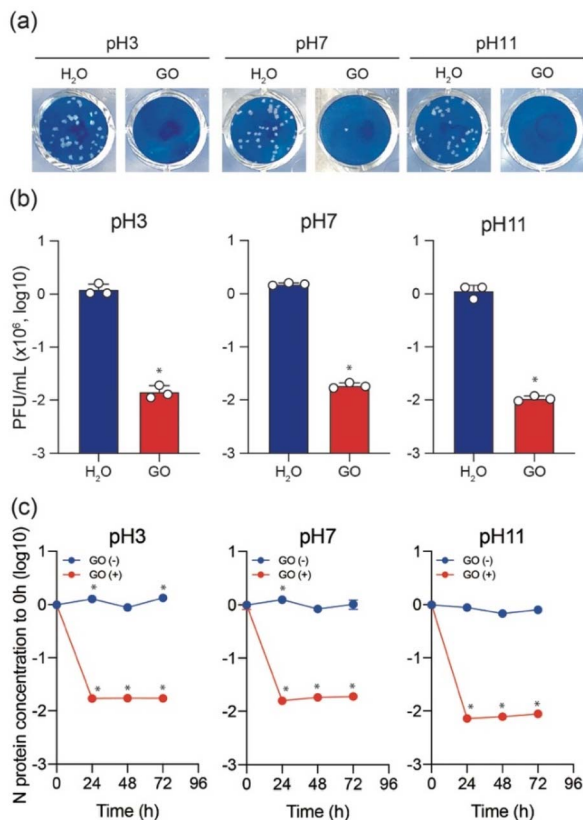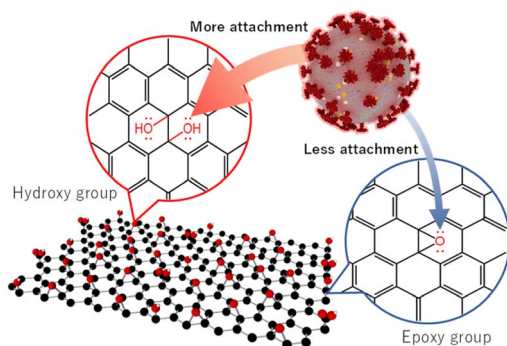

Fig. 2 Antiviral effects of pH-dependent GO nanosheets on Delta SARS-CoV-2 strains. (a and b) Anti-SARS-CoV-2 activity in the presence (red) or absence (blue, H2O) of GO (100 μg mL⁻¹) at three different pH using plaque assay. Panel (a) shows representative pictures of plaque assay. Panel (b) shows representative plaque assay data with average ± standard deviation (SD). All experiments were performed in triplicate. Statistical significance was assessed using a two-sided paired *t*-test. *$p < 0.05$ compared with H2O. (c) Results of N protein ELISA with (red) and without (blue) the presence of GO. The average of biological triplicate is shown. Statistical comparisons were made using a two-sided paired *t*-test. *$p < 0.01$ compared to each 0 h sample.

further ensure the pH effect of the GO dispersion on antiviral activity, ELISA was conducted to cause the destruction of N protein in the presence of GO (3), GO (7), and GO (11) after incubation for 0, 24, 48, and 72 h, respectively. The results are shown on a log scale in Fig. 2c.

Clearly, N protein concentration was stable over time in the absence of GO, and the variations at pH 3, 7, and 11 conditions are insignificant. However, a significant decline in the N protein's concentration is observed in the first 24 h upon treating the virus stock with GO under all pH conditions. As expected, the results also support the increasing order of GO (7) < GO (3) < GO (11) for N protein destruction. It should be noted that in the current work, 1 mg mL⁻¹ GO solutions with different pH (also a solution without GO) were diluted to 0.1 mg mL⁻¹ in a virus dilution buffer [20 mM HEPES, 1% nonessential amino acid, 1% penicillin-streptomycin in DMEM (low glucose)] with the virus stock. Besides, DMEM (low glucose) medium includes phenol red that changes color depending on pH. We always saw the red color of the medium, which indicates no significant change in pH in the virus-GO mixture. After 1 h of incubation, GO was pelleted down in the mixture by centrifugation and the supernatant was used for infection into VeroE6/TMPRSS2 cells to examine the effect of GO on virus inhibition. Without GO (only different pH solutions with the same experimental procedure), SARS-CoV-2 still caused the formation of plaques, showing these experimental conditions to be significant for observing virus infectivity and the effect of GO.

The above observations confirm that GO (11) shows a higher anti-SARS-Cov-2 response than those of GO (3) and GO (7). GO prepared using a modified Hummers oxidation route from a graphite precursor is associated with the appearance of a large number of epoxide functional groups in the basal plane and carboxyl groups at the edge, which is a remarkable feature of GO.[24] However, the functional sites and the overall charges of GO can be modified by changing the pH of the GO dispersion. In a lower pH GO dispersion, the epoxy groups are much more stable in the protonated environment. Also, through a molecular dynamics simulation study C.-J. Shih and co-workers suggested that at low pH, the carboxyl groups are protonated such that the GO sheets become less hydrophilic and form a stable GO–water–GO sandwich-like structure.[25] On the other hand, at higher pH, the epoxy groups of the GO dispersion are changed to hydroxyl groups. The change of functional groups between epoxide and hydroxyl on the graphene oxide is associated with the bonding nature of linking carbon atoms as well. This results in a significant local structural distortion, including changes in associated bond lengths, altering the electrostatic characteristics of the involved atomic sites and the net surface charge of GO.[26] The charges on the O(epoxy) and O(hydroxyl) atoms are −0.36e and −0.70e, respectively.[27] Therefore, GO dispersions having a higher percentage of hydroxyls show better elastic properties towards positive particles. In addition, in a low pH environment, the ionized COO^- groups are gradually protonated, leading to a decrease in the overall negative charge of the GO. However, at higher pH, carboxyl groups are deprotonated, thus increasing the negative value of zeta potential. The zeta potentials of GO (3) and GO (11) are reported to be −24.90 and

Scheme 2 Functional groups of GO responsible for the attachment to and inactivation of SARS-CoV-2.

−52.20 mV, respectively which represent an overall charge decrease to a negative value, increasing the pH of GO.[28] Therefore, better adsorption of positively charged virus particles is expected for GO (11) along with the presence of a large number of surface hydroxyl groups and a much lower net negative charge in the zeta potential, which is reflected in the plaque assay and ELISA of SARS-CoV-2 inactivation.[6,12]

Furthermore, along with a large number of –OH groups in GO (11), it might have more tendency to show H-bonding which facilitates the attachment of GO (11) and virus particles. Therefore, we propose that the functional sites of GO (11) facilitate the attachment to the virus particles followed by their inactivation compared to those of GO (3)/GO (7), resulting in more virus inactivation (Scheme 2).

In summary, GO nanosheet dispersions at three different conditions including pH 3, 7, and 11 are applied to optimize the suppression of SARS-CoV-2. Both the plaque assay and the quantification of the N protein ELISA suggest that GO (11) has better performance toward SARS-CoV-2 compared to GO (3) and GO (7). The higher SARS-CoV-2 inactivation can be ascribed to the better attachment between the virus particles and GO (11). We believe that the current findings will provide further understanding and important guidelines for the implementation of GO-based infrastructure with/post-COVID-19 society.

Author contributions

S. H., Y. S., and T. I. designed the study and conceived the main conceptual ideas. M. S. I., M. F., and R. T. prepared and characterized the graphene oxide samples. M. N, K. S. and K. Y. provided the resources and collected the data. M. J. H. did the N protein ELISA experiment. M. S. I. and N. N. R. interpreted the results and prepared the original draft manuscript. S. H., Y. S., and T. I. revised the manuscript critically for important intellectual content. All authors discussed the results and commented on the manuscript.

Conflicts of interest

There are no conflicts to declare.

Notes and references

1 *COVID-19 Dashboard by the Center for Systems Science and Engineering (CSSE)*, Johns Hopkins University (JHU), https://coronavirus.jhu.edu/map.html.
2 P. Zhou, X.-L. Yang, X.-G. Wang, B. Hu, L. Zhang, W. Zhang, H.-R. Si, Y. Zhu, B. Li, C.-L. Huang, H.-D. Chen, J. Chen, Y. Luo, H. Guo, R.-D. Jiang, M.-Q. Liu, Y. Chen, X.-R. Shen, X. Wang, X.-S. Zheng, K. Zhao, Q.-J. Chen, F. Deng, L.-L. Liu, B. Yan, F.-X. Zhan, Y.-Y. Wang, G.-F. Xiao and Z.-L. Shi, *Nature*, 2020, **579**, 270–273.
3 V. Palmieri and M. Papi, *Nano Today*, 2020, **33**, 100883.
4 A. K. Srivastava, N. Dwivedi, C. Dhand, R. Khan, N. Sathish, M. K. Gupta, R. Kumar and S. Kumar, *Mater. Today Chem.*, 2020, **18**, 100385.
5 G. B. Ramaiah, A. Tegegne and B. Melese, *Mater. Today: Proc.*, 2021, **47**, 4357–4363.
6 M. Fukuda, M. S. Islam, R. Shimizu, H. Nasser, N. N. Rabin, Y. Takahashi, Y. Sekine, L. F. Lindoy, T. Fukuda, T. Ikeda and S. Hayami, *ACS Appl. Nano Mater.*, 2021, **4**, 11881–11887.
7 J. Yagyu, M. S. Islam, Y. Shudo, M. Fukuda, H. Ushijima, J. Ohyama, S. Ida, L. F. Lindoy and S. Hayami, *ACS Appl. Energy Mater.*, 2021, **4**, 6296–6301.
8 Y. Shudo, M. S. Islam, M. R. Karim, N. N. Rabin, K. Wakata, R. Ohtani, M. Nakamura, L. F. Lindoy and S. Hayami, *Global Challenges*, 2017, **1**, 1700054.
9 M. S. Islam, J. Yagyu, Y. Sekine, S. Sawa and S. Hayami, *Mater. Adv.*, 2022, **3**, 3418–3422.
10 S. Islam Md, Y. Shudo and S. Hayami, *Bull. Chem. Soc. Jpn.*, 2022, **95**, 1–25.
11 J. Yagyu, M. S. Islam, H. Yasutake, H. Hirayama, H. Zenno, A. Sugimoto, S. Takagi, Y. Sekine, S.-I. Ohira and S. Hayami, *Bull. Chem. Soc. Jpn.*, 2022, **95**, 862–870.
12 M. A. Unal, F. Bayrakdar, H. Nazir, O. Besbinar, C. Gurcan, N. Lozano, L. M. Arellano, S. Yalcin, O. Panatli, D. Celik, D. Alkaya, A. Agan, L. Fusco, S. Suzuk Yildiz, L. G. Delogu, K. C. Akcali, K. Kostarelos and A. Yilmazer, *Small*, 2021, **17**, 2101483.
13 H. He, J. Klinowski, M. Forster and A. Lerf, *Chem. Phys. Lett.*, 1998, **287**, 53–56.
14 A. Lerf, H. He, M. Forster and J. Klinowski, *J. Phys. Chem. B*, 1998, **102**, 4477–4482.

15 S. Stankovich, R. D. Piner, S. T. Nguyen and R. S. Ruoff, *Carbon*, 2006, **44**, 3342–3347.

16 T. Taniguchi, S. Kurihara, H. Tateishi, K. Hatakeyama, M. Koinuma, H. Yokoi, M. Hara, H. Ishikawa and Y. Matsumoto, *Carbon*, 2015, **84**, 560–566.

17 A. Saito, T. Irie, R. Suzuki, T. Maemura, H. Nasser, K. Uriu, Y. Kosugi, *et al.*, *Nature*, 2022, **602**, 300–306.

18 R. Suzuki, D. Yamasoba, I. Kimura, L. Wang, M. Kishimoto, J. Ito, Y. Morioka, N. Nao, H. Nasser, K. Uriu, Y. Kosugi, M. Tsuda, Y. Orba, M. Sasaki, R. Shimizu, R. Kawabata, K. Yoshimatsu, H. Asakura, M. Nagashima, K. Sadamasu, K. Yoshimura, H. Sawa, T. Ikeda, T. Irie, K. Matsuno, S. Tanaka, T. Fukuhara and K. Sato, *Nature*, 2022, **603**, 700–705.

19 D. Yamasoba, I. Kimura, H. Nasser, Y. Morioka, N. Nao, J. Ito, K. Uriu, M. Tsuda, J. Zahradnik, K. Shirakawa, *et al.*, *Cell*, 2022, **185**, 2103–2115.

20 M. Fukuda, M. S. Islam, Y. Shudo, J. Yagyu, L. F. Lindoy and S. Hayami, *Chem. Commun.*, 2020, **56**, 4364–4367.

21 H. Takehira, M. S. Islam, M. R. Karim, Y. Shudo, R. Ohtani, L. F. Lindoy, T. Taniguchi, M. Osada and S. Hayami, *ChemistrySelect*, 2017, **2**, 6941–6944.

22 A. M. Dimiev, L. B. Alemany and J. M. Tour, *ACS Nano*, 2013, **7**, 576–588.

23 I. Kimura, D. Yamasoba, T. Tamura, N. Nao, T. Suzuki, Y. Oda, S. Mitoma, J. Ito, H. Nasser, J. Zahradnik, K. Uriu, S. Fujita, Y. Kosugi, L. Wang, M. Tsuda, M. Kishimoto, H. Ito, R. Suzuki, R. Shimizu, M. M. Begum, K. Yoshimatsu, K. T. Kimura, J. Sasaki, K. Sasaki-Tabata, Y. Yamamoto, T. Nagamoto, J. Kanamune, K. Kobiyama, H. Asakura, M. Nagashima, K. Sadamasu, K. Yoshimura, K. Shirakawa, A. Takaori-Kondo, J. Kuramochi, G. Schreiber, K. J. Ishii, T. Hashiguchi, T. Ikeda, A. Saito, T. Fukuhara, S. Tanaka, K. Matsuno and K. Sato, *Cell*, 2022, **185**, 3992–4007.

24 M. R. Karim, M. S. Islam, K. Hatakeyama, M. Nakamura, R. Ohtani, M. Koinuma and S. Hayami, *J. Phys. Chem. C*, 2016, **120**, 21976–21982.

25 C.-J. Shih, S. Lin, R. Sharma, M. S. Strano and D. Blankschtein, *Langmuir*, 2012, **28**, 235–241.

26 F. Abbasi, J. Karimi-Sabet, C. Ghotbi, Z. Abbasi, S. A. Mousavi and N. Amini, *Sci. Iran.*, 2017, **24**, 3554–3559.

27 A. J. P. Neto, V. V. Chaban and E. E. Fileti, *Phys. Chem. Chem. Phys.*, 2017, **19**, 32333–32340.

28 B. Konkena and S. Vasudevan, *J. Phys. Chem. Lett.*, 2012, **3**, 867–872.